Photonic band gaps for arrays of perfectly conducting cylinders

N.A. Nicorovici and R.C. McPhedran
Department of Theoretical Physics, School of Physics, University of Sydney, New South Wales 2006, Australia

L.C. Botten
School of Mathematical Sciences, University of Technology Sydney, New South Wales 2007, Australia
(Received 13 March 1995)

We study the propagation of electromagnetic waves through arrays of perfectly conducting cylinders for both fundamental polarization cases s and p. We use a generalized Rayleigh identity method and show that for p polarization the fundamental band defines an effective refractive index not in keeping with electrostatics. We exhibit the photonic band structures for very dilute arrays, where they tend towards the expected free-propagation form. We also study them for arrays approaching touching, where very interesting differences between s and p polarization behavior are manifest.

PACS number(s): 41.20.Jb, 42.25.Fx, 71.25.Cx

I. INTRODUCTION

The idea that singly, doubly, and triply periodic dielectric lattices can be designed to possess photonic band gaps has attracted wide attention, both theoretically and experimentally [1,2]. The absence of electromagnetic modes inside a photonic band gap can lead to unusual physical phenomena. Thus, atoms or molecules embedded in such a structure, called a dielectric crystal, can be locked in an excited state if the energy of this state, relative to the ground state, falls within the photonic band gap. In this case, the atoms (or molecules) are also expected to exhibit an anomalous Lamb shift. At the same time, in a dielectric crystal new types of electron-photon interactions appear leading to a specific behavior of light. However, the three-dimensional dielectric crystals have a quite complex structure and their fabrication is difficult, particularly for the optical and near-infrared regions. A promising type of photonic band-gap materials consists of arrays of dielectric material periodic along two axes (x and y) and homogeneous in the third direction (z). Although this structure reflects only in-plane incident waves, there are several applications where this is sufficient [3].

The most widely used theoretical approach in calculating the photonic band structures relies on the treatment of the full vector Maxwell equations by means of plane-wave expansions [4–6]. In this method, the field and the dielectric constant are expanded in infinite series of plane waves, so that the problem is reduced to an infinite-dimensional eigenvalue problem. Due to the fact that the plane-wave expansions converge slowly, this method requires a large number of terms in the series, in order to obtain accurate numerical results. By truncating the series, the high-frequency components are removed. Also, the dielectric constant is poorly estimated near spatial discontinuities [7–9]. For metallic systems at high frequencies the dielectric constant may exibit a very large imaginary part and the plane-wave expansions become impractical [10]. The numerical techniques used to avoid these difficulties still require the evaluation of large determinants by complicated and time consuming algorithms.

In a series of papers we have extended Rayleigh's technique [11] from electrostatic to full electromagnetic problems, for singly [12–14], doubly [15–17], and triply [18] periodic systems. Rayleigh's method involves a set of lattice sums which consists of sums over terms with a function evaluated at each lattice point, and the evaluation of lattice sums is the most important and subtle part of this technique. The main reason is that the definition of lattice sums involves conditionally converging series over the direct lattice, and a direct evaluation is thus impractical if high accuracy is needed. The lattice sums involved in our method are represented in terms of absolutely converging series over the reciprocal lattice, and in contrast to the method used by Ewald [19], these series may be accelerated by successive integrations to any order. By introducing the lattice sums, we obtain a representation of the Green's function in terms of a rapidly convergent Neumann series. Also, the representation in terms of absolutely converging series allows us to have some physical insight into the analytic properties of the lattice sums. For the coefficients in the multipole expansions of fields we have obtained a generalized Rayleigh identity. Our method is capable of studying, numerically and analytically, problems in which the dielectric constant is piecewise constant and may take finite or infinite values. Generally, our method may be applied when the cylinders are composed of an arbitrary number of coaxial circular shells filled with materials having different complex dielectric constants.

In this paper we study the electromagnetic properties of a two-dimensional photonic band-gap material, structured as an array of perfectly conducting cylinders. For isotropic and homogeneous matrix and inclusions, Rayleigh's theory applies equally well to the computation of effective dielectric constant or effective conductivity of a composite. Here, we use the term "perfectly conducting cylinders" as a more familiar term, substituting for

what are precisely "infinite refractive index cylinders."

We will study the rapidity of convergence of our method, showing that for dilute arrays of cylinders only a small number of terms in series is needed, while for closely packed arrays the number of terms increases. We will also use our formulation to study the question of homogenization [20–26], i.e., the attribution of an effective refractive index to our system consisting of cylinders of a specified (infinite) refractive index separated by a matrix of another refractive index. The formulation we use has the potential to yield new insights into the conditions for the validity of the homogenization process, since it provides a solution of Maxwell's equations for this system, but has at its core an electrostatic formulation yielding the homogenized solution.

Some of the ideas presented here can also be found in [27] and [28], where the problems are discussed of scattering by a finite set of parallel cylinders, of arbitrary cross section [27] or circular [28], randomly distributed in a finite region of space.

II. THEORY

We consider the following diffraction problem: a plane electromagnetic wave propagates through a periodic array of perfectly conducting cylinders embedded in a host medium. The cylinders are of infinite length and radius a, with the axes parallel to the z axis. The incident plane wave is characterized by its wavelength λ and the wave vector $|\mathbf{k}_0| = 2\pi/\lambda$, perpendicular to the axes of the cylinders.

The geometry of the array is defined by the fundamental translation vectors $\widehat{\mathbf{e}}_1$ and $\widehat{\mathbf{e}}_2$, the origin being one node of the array (see Fig. 1). These vectors are not necessarily orthogonal, nor are their lengths necessarily equal. Thus, the vectors from the origin of coordinates to the pth node of the array are specified by a set of two integers:

$$\mathbf{R}_p = p_1\widehat{\mathbf{e}}_1 + p_2\widehat{\mathbf{e}}_2 \quad , \tag{1}$$

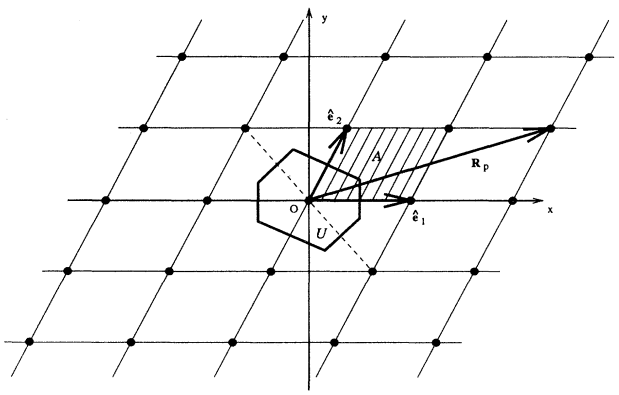

FIG. 1. The two-dimensional lattice. The primitive cell A (dashed area) is defined by the fundamental translation vectors $\widehat{\mathbf{e}}_1$ and $\widehat{\mathbf{e}}_2$. We also mark the unit cell U (the Wigner-Seitz cell).

where $p = (p_1, p_2) \in \mathbb{Z}^2$. We denote by $\mathcal{A}$ the primitive cell of the array and by $A = |\widehat{\mathbf{e}}_1 \times \widehat{\mathbf{e}}_2|$ the area of $\mathcal{A}$. The primitive cell of the reciprocal array is defined by the vectors

$$\widehat{\mathbf{u}}_1 = 2\pi\frac{\widehat{\mathbf{e}}_2 \times \widehat{\mathbf{a}}}{A} \ , \ \widehat{\mathbf{u}}_2 = 2\pi\frac{\widehat{\mathbf{a}} \times \widehat{\mathbf{e}}_1}{A} \ , \tag{2}$$

where $\widehat{\mathbf{a}} = (\widehat{\mathbf{e}}_1 \times \widehat{\mathbf{e}}_2)/A$. The vectors from the origin to the hth node of the reciprocal array have the form

$$\mathbf{K}_h = h_1\widehat{\mathbf{u}}_1 + h_2\widehat{\mathbf{u}}_2 \ , \ h = (h_1, h_2) \in \mathbb{Z}^2. \tag{3}$$

In the case when the host medium is an isotropic homogeneous dielectric in which the electromagnetic wave has the wave number k, the equations for the components of the electric and magnetic fields decouple and each field component satisfies the Helmholtz equation. The wave vectors $\mathbf{k}_0$ and $\mathbf{k}$ are parallel to the xy plane, therefore the components of the fields are independent of z. At the same time, the problem can be reduced to solving two independent problems: (i) for the s polarization (or TM), when the electric field is along the z axis perpendicular to the plane of propagation, and (ii) for the p polarization (or TE), when the electric field is parallel to the plane of propagation [29].

Consequently, the field components are given by the solutions of the two-dimensional Helmholtz equation:

$$\left(\nabla^2 + k^2\right) V = 0, \tag{4}$$

where $V = E_z, H_z$ for the s, p polarizations, respectively, with the boundary conditions at the surface (∂C_p) of each cylinder:

$$V|_{\partial C_p} = 0 \ , \ s \ \text{polarization}, \tag{5}$$

$$\left.\frac{\partial V}{\partial \mathbf{n}}\right|_{\partial C_p} = 0 \ , \ p \ \text{polarization}, \tag{6}$$

respectively, the field component and its normal derivative vanishing. In addition, the fields are also required to satisfy a quasiperiodicity condition:

$$V(\mathbf{r} + \mathbf{R}_p) = e^{i\mathbf{k}_0\cdot\mathbf{R}_p} V(\mathbf{r}). \tag{7}$$

The quasiperiodicity condition follows from the Bloch theorem, stating that the field on the pth cylinder depends explicitly on the cylinder position ($\mathbf{R}_p$) through the phase factor $\exp(i\mathbf{k}_0 \cdot \mathbf{R}_p)$ [30].

Therefore, we have to solve a Dirichlet problem for the s polarization and a Neumann problem for the p polarization. For both problems, the Green's function is the elementary solution of the inhomogenous equation:

$$\left(\nabla^2 + k^2\right) G = -2\pi \sum_p \delta(\mathbf{r} - \mathbf{R}_p - \boldsymbol{\rho}) e^{i\mathbf{k}_0\cdot\mathbf{R}_p}, \tag{8}$$

and satisfies the quasiperiodicity conditions

$$G(\mathbf{r} + \mathbf{R}_p, \boldsymbol{\rho}) = e^{i\mathbf{k}_0\cdot\mathbf{R}_p} G(\mathbf{r}, \boldsymbol{\rho}), \tag{9}$$

$$G(\mathbf{r}, \boldsymbol{\rho} + \mathbf{R}_p) = e^{-i\mathbf{k}_0\cdot\mathbf{R}_p} G(\mathbf{r}, \boldsymbol{\rho}). \tag{10}$$

When the vector $\mathbf{r} - \boldsymbol{\rho}$ is restricted to the unit cell cen-

tered at the origin of coordinates, the Green's function is unique and takes a form [16,17] corresponding to a source within the central unit cell and a sum of the sources within other unit cells:

$$G(\mathbf{r},\boldsymbol{\rho}) = -\frac{\pi}{2}Y_0(k|\mathbf{r}-\boldsymbol{\rho}|) - \frac{\pi}{2}\sum_{\ell=-\infty}^{\infty} S_\ell^Y(k,\mathbf{k}_0)J_\ell(k|\mathbf{r}-\boldsymbol{\rho}|)e^{-i\ell\alpha}, \quad (11)$$

where, if $r > \rho$, $\alpha = \arg(\mathbf{r}-\boldsymbol{\rho})$. Also, J, Y are Bessel functions of the first and second kind, respectively. The coefficients S_ℓ^Y are lattice sums given by the formula [16,17]

$$S_\ell^Y(k,\mathbf{k}_0)J_{\ell+m}(k) = -\left[Y_m(k) + \frac{1}{\pi}\sum_{n=1}^{m}\frac{(m-n)!}{(n-1)!}\left(\frac{2}{k}\right)^{m-2n+2}\right]\delta_{\ell,0} - i^\ell\frac{4}{A}\sum_h\left(\frac{k}{Q_h}\right)^m\frac{J_{\ell+m}(Q_h)}{Q_h^2-k^2}e^{i\ell\theta_h}, \quad (12)$$

where $\mathbf{Q}_h = \mathbf{k}_0 + \mathbf{K}_h$, $\theta_h = \arg(\mathbf{Q_h})$, and m is an arbitrary non-negative integer used to improve the convergence of the series in (12). Since the Green's function (11) is unique, the form (12) for the lattice sums S_ℓ^Y is also unique.

In polar coordinates, the solution of (4) has the general form

$$V(r,\theta) = \sum_{\ell=-\infty}^{\infty}\left[A_\ell^{(\gamma)}J_\ell(kr) + B_\ell^{(\gamma)}Y_\ell(kr)\right]e^{i\ell\theta}, \quad (13)$$

where γ labels the polarization (s or p). The coefficients $A_\ell^{(\gamma)}$ and $B_\ell^{(\gamma)}$ are related by $A_\ell^{(\gamma)} = -M_\ell^{(\gamma)}B_\ell^{(\gamma)}$, with $M_\ell^{(\gamma)}$ given by the boundary conditions (5) and (6):

$$M_\ell^{(s)} = \frac{Y_\ell(ka)}{J_\ell(ka)}, \quad M_\ell^{(p)} = \frac{Y_\ell'(ka)}{J_\ell'(ka)}, \quad (14)$$

the prime indicating the derivative of the corresponding function.

By means of (11) and (13), following the method developed by Lord Rayleigh [11] for static problems and extended to dynamic problems [15–17], we obtain the coefficients $B_\ell^{(\gamma)}$ from the generalized Rayleigh identity [17]:

$$M_\ell^{(\gamma)}B_\ell^{(\gamma)} + \sum_{m=-\infty}^{\infty}(-1)^{\ell+m}S_{m-\ell}^Y(k,\mathbf{k}_0)B_m^{(\gamma)} = 0. \quad (15)$$

The values k for which the determinant of the homogeneous system (15) vanishes are the eigenvalues of the Helmholtz equation (4), i.e., the wave numbers of the propagating waves. In the coordinate system k versus $\mathbf{k}_0$, the set of trajectories of eigenvalues when the incident wave vector $\mathbf{k}_0$ follows the boundary of the first irreducible Brillouin zone represents the photonic band structure of the physical system. The lowest values of k form an "acoustic band," if $k \to 0$ when $\mathbf{k}_0 \to 0$ [30]; this terminology *does not* mean we refer to an actual acoustic wave, but rather to an electromagnetic wave whose dispersion curve resembles that of the acoustic band in phonon dispersion theory.

The null vectors $\{B_\ell^{(\gamma)}(k)\}$ corresponding to each allowed wave number k define the field component V, through Eqs. (13) and (14). In turn, V defines completely the electric and magnetic fields through

$$\mathbf{E} = (0,0,V), \quad \mathbf{H} = \frac{i}{k_0Z_0}\hat{\mathbf{z}}\times\nabla V, \quad (16)$$

for s polarization, and

$$\mathbf{H} = (0,0,V), \quad \mathbf{E} = -\frac{iZ_0}{k_0}\hat{\mathbf{z}}\times\nabla V, \quad (17)$$

for p polarization. Here, $\hat{\mathbf{z}}$ represents the unit vector along the z axis and $Z_0 = \sqrt{\mu_0/\varepsilon_0}$ is the free space impedance.

III. THE QUASISTATIC LIMIT AND HOMOGENIZATION

To compute the set of dispersion curves, we concentrate on general values of $\mathbf{k}_0$ avoiding values invariant under any of the symmetry operations from the lattice symmetry group. We may then use the lattice sums as defined in (12). If the Bloch momentum $\mathbf{k}_0$ is invariant under some of the symmetry operations from the lattice symmetry group, we have to analyze in detail the behavior of the lattice sums in such a special case.

Thus, for any lattice a point of high symmetry is $\mathbf{k}_0 = 0$, and in the system k versus $\mathbf{k}_0$, we may distinguish two cases [30]: (i) $\mathbf{k}_0 = 0$ and $k \neq 0$, giving the central point on each optical band, and (ii) $\mathbf{k}_0 \to 0$ and $k = \alpha k_0$ for the acoustic band. In the first case, the lattice sums are simply obtained by replacing $\mathbf{Q}_h$ with $\mathbf{K}_h$ in (12). The second case represents the quasistatic limit when the linear system (15) takes the form of Rayleigh's identity for the relevant lattice in an electrostatic field. To explain the meaning of the coefficient α we have to take into account that, for the present problem, $k_z = 0$. According to Bloch's theorem the phase difference of V between $x = -d/2$ and $x = d/2$ is

$$\Delta\Phi = k_0 d = \mathcal{N}kd, \quad (18)$$

an equation defining the effective phase refractive index ($\mathcal{N}$) of the array. Hence

$$\mathcal{N} = \frac{1}{\alpha} = \left.\frac{dk_0}{dk}\right|_{k=0}. \quad (19)$$

The question of constructing equivalent continuous media to composite materials is a very old one in physics, being linked with early work on the relationship between atomic and continuum models, by Faraday, Clausius, Mossotti, Maxwell, Lorenz, Lorentz, Rayleigh, Maxwell-Garnett, and others [31]. It is also a topic of much recent work in applied mathematics, where it tends to be referred to as homogenization theory [20–26].

In order to study the quasistatic limit and the corre-

sponding expression of the effective refractive index $\mathcal{N}$, we have to find how the coefficients $B_\ell^{(\gamma)}$ in (13) depend on k. First, we consider p polarization with the boundary conditions (6), so that the field component (13) takes the form

$$\begin{aligned} H_z(r,\theta) &= -\sum_{\ell=-\infty}^{\infty}\left[\frac{J_\ell(kr)}{J'_\ell(ka)}-\frac{Y_\ell(kr)}{Y'_\ell(ka)}\right]Y'_\ell(ka)B_\ell^{(p)}e^{i\ell\theta} \\ &= -\left[J_0(kr)\frac{Y'_0(ka)}{J'_0(ka)}-Y_0(kr)\right]B_0^{(p)} \\ &\quad -\sum_{\ell=1}^{\infty}\left[\frac{J_\ell(kr)}{J'_\ell(ka)}-\frac{Y_\ell(kr)}{Y'_\ell(ka)}\right] \\ &\quad \times Y'_\ell(ka)\left[B_\ell^{(p)}e^{i\ell\theta}+(-1)^\ell B_{-\ell}^{(p)}e^{-i\ell\theta}\right]. \end{aligned} \tag{20}$$

By substituting the expressions of Bessel functions and their derivatives for small arguments [32], we obtain

$$\begin{aligned} H_z(r,\theta) &\sim \left[\frac{1}{\pi}\left(\frac{2}{ka}\right)^2+\frac{2}{\pi}\ln(kr)\right]B_0^{(p)} \\ &\quad -ka\sum_{\ell=1}^{\infty}\frac{1}{\ell}\left[\left(\frac{r}{a}\right)^\ell+\left(\frac{a}{r}\right)^\ell\right] \\ &\quad \times\left(\widetilde{B}_\ell^{(p)}e^{i\ell\theta}+\widetilde{B}_{-\ell}^{(p)}e^{-i\ell\theta}\right), \end{aligned} \tag{21}$$

where $\widetilde{B}_\ell^{(p)} = Y'_\ell(ka)B_\ell^{(p)}$, with, for later use, $\widetilde{B}_0^{(p)} = Y'_0(ka)B_0^{(p)}$. From (17), we have the electric field given by the formula

$$\mathbf{E} = \widehat{\mathbf{z}}\times\nabla\Psi\ , \tag{22}$$

where we have denoted

$$\Psi(r,\theta) = -\frac{iZ_0}{k_0}H_z(r,\theta)\ . \tag{23}$$

In the quasistatic limit $k=\alpha k_0$, so that (23) may be written in the form

$$\begin{aligned} \Psi(r,\theta) &\sim -i\frac{\alpha Z_0}{\pi}\left[\left(\frac{2}{ka}\right)^2+2\ln(kr)\right]\frac{B_0^{(p)}}{k} \\ &\quad +i\alpha Z_0 a\sum_{\ell=1}^{\infty}\frac{1}{\ell}\left[\left(\frac{r}{a}\right)^\ell+\left(\frac{a}{r}\right)^\ell\right] \\ &\quad \times\left(\widetilde{B}_\ell^{(p)}e^{i\ell\theta}+\widetilde{B}_{-\ell}^{(p)}e^{-i\ell\theta}\right). \end{aligned} \tag{24}$$

In Rayleigh's theory for an array of perfectly conducting cylinders in an electrostatic field, the electric potential in the host medium is the solution of a Dirichlet problem for the Laplace equation, and the electric field has the form [11,33,34]

$$\mathbf{E} = -\nabla\varphi\ , \tag{25}$$

with

$$\varphi(r,\theta) = -\sum_{\ell=1}^{\infty}\left[\left(\frac{r}{a}\right)^\ell-\left(\frac{a}{r}\right)^\ell\right]\frac{b_\ell}{a^\ell}\cos(\ell\theta). \tag{26}$$

The same electric field is given by the solution of a Neumann problem for the Laplace equation. Now, the electric field is produced by a "magnetic" potential:

$$\mathbf{E} = \widehat{\mathbf{z}}\times\nabla\psi\ , \tag{27}$$

with

$$\psi(r,\theta) = -\sum_{\ell=1}^{\infty}\left[\left(\frac{r}{a}\right)^\ell+\left(\frac{a}{r}\right)^\ell\right]\frac{b_\ell}{a^\ell}\sin(\ell\theta). \tag{28}$$

We mention that the potentials $\varphi(r,\theta)$ and $\psi(r,\theta)$ form a Cauchy-Riemann pair, so that $\nabla\varphi = -\widehat{\mathbf{z}}\times\nabla\psi$. Also, the coefficients b_ℓ are assumed to be real, and the applied electric field is oriented along the x axis or y axis. For an arbitrary orientation of the applied field, the coefficients b_ℓ are complex, and we obtain

$$\psi(r,\theta) = \frac{i}{2}\sum_{\ell=1}^{\infty}\left[\left(\frac{r}{a}\right)^\ell+\left(\frac{a}{r}\right)^\ell\right]\frac{1}{a^\ell}\left(b_\ell^* e^{i\ell\theta}-b_\ell e^{-i\ell\theta}\right), \tag{29}$$

where the asterisk denotes complex conjugation. The corresponding expression for φ is

$$\varphi(r,\theta) = -\frac{1}{2}\sum_{\ell=1}^{\infty}\left[\left(\frac{r}{a}\right)^\ell-\left(\frac{a}{r}\right)^\ell\right]\frac{1}{a^\ell}\left(b_\ell^* e^{i\ell\theta}+b_\ell e^{-i\ell\theta}\right). \tag{30}$$

In the case of p polarization we have a Neumann problem for the Helmholtz equation, and for small k we have obtained Eq. (24). The comparison between (24) and (29) suggests that, for $\ell\neq 0$, the coefficients $\widetilde{B}_\ell^{(p)}$, to leading order, are independent of k. Also, in order to remove the logarithmic divergence in (24), we have to assume that the coefficient $B_0^{(p)}$ is proportional to k^2. The first term in the coefficient of $\widetilde{B}_0^{(p)}$, proportional to $1/k$, does not depend on r and, therefore, does not contribute to the electric field in (22). It corresponds to a surface current on each cylinder.

By substituting the coefficients $\widetilde{B}_\ell^{(p)}$ in (15), after some algebraic manipulations, we obtain the homogeneous system

$$\sum_{m=-\infty}^{\infty}\left[\delta_{m\ell}+(-1)^{\ell+m}\frac{J'_\ell(ka)}{Y'_m(ka)}S^Y_{m-\ell}(k,\mathbf{k}_0)\right]\widetilde{B}_m^{(p)} = 0. \tag{31}$$

Here, $\delta_{m\ell}$ represents the Kronecker symbol, and $-\infty\le\ell\le\infty$. Next, we use the dipole approximation. This means truncating the system (31) to $-1\le\ell,m\le 1$. For small arguments the ratios of the derivatives of Bessel functions become [32]

$$\begin{aligned} &\frac{J'_1(ka)}{Y'_1(ka)}\sim\pi\left(\frac{ka}{2}\right)^2\ ,\quad \frac{J'_1(ka)}{Y'_0(ka)}\sim\pi\frac{ka}{4}\ , \\ &\frac{J'_0(ka)}{Y'_1(ka)}\sim-\pi\frac{(ka)^3}{4}\ ,\quad \frac{J'_0(ka)}{Y'_0(ka)}\sim-\pi\left(\frac{ka}{2}\right)^2. \end{aligned} \tag{32}$$

For the derivatives of Bessel functions of negative order we use the relations $J'_{-\ell}(z) = (-1)^{\ell} J_{\ell}(z)$ and $Y'_{-\ell}(z) = (-1)^{\ell} Y_{\ell}(z)$.

From (12) we obtain the expressions of the lattice sums S_{ℓ}^{Y}, for $\mathbf{k}_0 \to 0$ and $k = \alpha k_0$ [where for analytic calculations it is convenient to choose $m = 0$ in (12)]. In this limit $Q_h \sim K_h$ and $k \ll K_h$, $\forall h \neq (0,0)$, while $\mathbf{Q}_0 = \mathbf{k}_0$. The only lattice sums involved in the dipole approximation are the lattice sums of order $\ell = 0, 1, 2$:

$$S_0^Y \sim -\frac{4}{A}\frac{1}{k_0^2(1-\alpha^2)} - \frac{2}{\pi}\ln k - \frac{4}{A}\sum_{h\neq 0}\frac{J_0(K_h)}{K_h^2}, \quad (33)$$

$$S_1^Y \sim -i\frac{4}{A}\frac{1}{k_0^2\alpha(1-\alpha^2)}e^{i\theta_0} - i\frac{8}{kA}\sum_{h\neq 0}\frac{J_1(K_h)}{K_h^2}e^{i\theta'_h}, \quad (34)$$

$$S_2^Y \sim \frac{4}{A}\frac{1}{k_0^2\alpha^2(1-\alpha^2)}e^{2i\theta_0} + \frac{32}{k^2A}\sum_{h\neq 0}\frac{J_2(K_h)}{K_h^2}e^{2i\theta'_h}, \quad (35)$$

where θ_0 is the polar angle of $\mathbf{k}_0$, and $\theta'_h = \arg(\mathbf{K}_h)$. Generally, for any array the series in (33) is convergent and gives a constant, while the series in (34) vanishes identically. The series in (35) vanishes in the case of a square or hexagonal array. In the system (31) the logarithmic term from (33) is multiplied by $J'_{\ell}(ka)/Y'_{\ell}(ka)$, therefore, in the limit $k \to 0$, it does not contribute to the coefficients of $\widetilde{B}_m^{(p)}$ in (31). In order to use the simplest form of the lattice sum S_2^Y, in what follows we will restrict our calculations to square or hexagonal arrays. Consequently, the dominant terms for the lattice sums (33)–(35) are

$$S_0^Y \sim -\frac{4}{A}\frac{1}{k_0^2(1-\alpha^2)}, \quad (36)$$

$$S_1^Y \sim -i\frac{4}{A}\frac{1}{k_0^2\alpha(1-\alpha^2)}e^{i\theta_0}, \quad (37)$$

$$S_2^Y \sim \frac{4}{A}\frac{1}{k_0^2\alpha^2(1-\alpha^2)}e^{2i\theta_0}. \quad (38)$$

The lattice sums of negative order are given by the complex conjugate of lattice sums of positive order [16]:

$$S_{-\ell}^Y(k, \mathbf{k}_0) = S_{\ell}^{Y^*}(k, \mathbf{k}_0). \quad (39)$$

Finally, the system (31) reduces to

$$\begin{bmatrix} 1 - f\frac{\alpha^2}{1-\alpha^2} & -f\frac{e^{i\theta_0}}{a(1-\alpha^2)} & -f\frac{e^{2i\theta_0}}{1-\alpha^2} \\ f\frac{\alpha^2 a e^{-i\theta_0}}{1-\alpha^2} & 1 + f\frac{\alpha^2}{1-\alpha^2} & f\frac{\alpha^2 a e^{i\theta_0}}{1-\alpha^2} \\ -f\frac{e^{-2i\theta_0}}{1-\alpha^2} & -f\frac{e^{-i\theta_0}}{a(1-\alpha^2)} & 1 - f\frac{\alpha^2}{1-\alpha^2} \end{bmatrix} \begin{bmatrix} \widetilde{B}_{-1}^{(p)} \\ i\widetilde{B}_0^{(p)}/k_0 \\ \widetilde{B}_1^{(p)} \end{bmatrix} = 0, \quad (40)$$

with $f = \pi a^2/A$. The unknown $\widetilde{B}_0^{(p)}/k_0$ is finite because, for small k_0, $Y'_0(ka) = -Y_1(ka) \sim 2/(\pi ka)$ and we have assumed that $B_0^{(p)} \sim k^2$, so that $\widetilde{B}_0^{(p)} \sim k = \alpha k_0$. Also, even if $\widetilde{B}_0^{(p)}$ depends on α, the value of α is fixed by the condition that the determinant of the homogeneous linear system (40) has to vanish.

The determinant of the system (40) is

$$\Delta^{(p)} = (1-f^2)(1-\alpha^2)[1-\alpha^2(1+f)], \quad (41)$$

and vanishes if $\alpha^2 = 1/(1+f)$. Hence, the effective dynamic refractive index of the array, in the dipole approximation, is

$$\mathcal{N}_d = (1+f)^{1/2}. \quad (42)$$

Also, the components of the normalized null vector have the form

$$\left|\widetilde{B}_{\pm 1}^{(p)}\right|^2 = \frac{1}{2+k_0^2a^2}, \quad \left|\widetilde{B}_0^{(p)}\right|^2 = \frac{k_0^2a^2}{2+k_0^2a^2}, \quad (43)$$

$$\widetilde{B}_0^{(p)} = i(k_0a)e^{-i\theta_0}\widetilde{B}_{-1}^{(p)} = i(k_0a)e^{i\theta_0}\widetilde{B}_1^{(p)}. \quad (44)$$

Note that, in the dipole approximation, these results are true for both the square and hexagonal arrays of circular cylinders, while for rectangular arrays and for the oblique array we would expect $\mathcal{N}_d$ to depend on the incidence angle θ_0. We have verified numerically the form (44) of the null vector by using a high order solution of (31) at low volume fractions, with small k_0.

In Table I we display numerical results confirming Eq. (42). $\mathcal{N}$ and N_∞ display converged numerical results, respectively, coming from Maxwell's equations, by means of (15), and electrostatics [33]. The fourth and sixth columns display solutions of the same equations in the dipole approximation, Eq. (42) for Maxwell's equations

TABLE I. The effective refractive index ($\mathcal{N}$) of a square array of perfectly conducting cylinders, for different area fractions ($f = \pi a^2$). The system (15) has been truncated to $-20 \leq \ell, m \leq 20$. We also display the dipole approximation ($\mathcal{N}_d$) as well as the corresponding results of electrostatics (N_∞ and N_d).

a	f	$\mathcal{N}$	$\mathcal{N}_d$	N_∞	N_d
0.26	0.212	1.1013	1.1011	1.2408	1.2407
0.30	0.283	1.1334	1.1326	1.3381	1.3373
0.34	0.363	1.1736	1.1676	1.4663	1.4631
0.38	0.454	1.2151	1.2051	1.6435	1.6311
0.42	0.554	1.2782	1.2467	1.9135	1.8672

and the Maxwell Garnett formula:

$$N_d = \left(\frac{1+f}{1-f}\right)^{1/2}, \tag{45}$$

for electrostatics. It can be seen that the dipole approximation is accurate for small area fractions, but loses accuracy with increasing area fraction. Note the clear difference between the effective dynamic refractive index ($\mathcal{N}$) and the refractive index (N_∞) derived from the effective static dielectric constant. Note also that the differences between the dipole approximation and the converged results are comparable for the results of Maxwell's equations and electrostatics.

In the case of s polarization, the Rayleigh identity (15) takes the form

$$\sum_{m=-\infty}^{\infty}\left[\delta_{m\ell}+(-1)^{\ell+m}\frac{J_\ell(ka)}{Y_m(ka)}S^Y_{m-\ell}(k,\mathbf{k}_0)\right]\widetilde{B}^{(s)}_m=0, \tag{46}$$

with $\widetilde{B}^{(s)}_m = Y_m(ka)B^{(s)}_m$. Now, the electric field is given by (13) and (5):

$$\begin{aligned}E_z(r,\theta) &= -\sum_{\ell=-\infty}^{\infty}\left[\frac{J_\ell(kr)}{J_\ell(ka)}-\frac{Y_\ell(kr)}{Y_\ell(ka)}\right]Y_\ell(ka)B^{(s)}_\ell e^{i\ell\theta}\\ &= -\left[J_0(kr)\frac{Y_0(ka)}{J_0(ka)}-Y_0(kr)\right]B^{(s)}_0\\ &\quad -\sum_{\ell=1}^{\infty}\left[\frac{J_\ell(kr)}{J_\ell(ka)}-\frac{Y_\ell(kr)}{Y_\ell(ka)}\right]\\ &\quad \times Y_\ell(ka)\left[B^{(s)}_\ell e^{i\ell\theta}+(-1)^\ell B^{(s)}_{-\ell}e^{-i\ell\theta}\right].\end{aligned} \tag{47}$$

and in the quasistatic limit becomes

$$\begin{aligned}E_z(r,\theta) &\sim \left[\frac{2}{\pi}\ln(r/a)\right]B^{(s)}_0\\ &\quad -\sum_{\ell=1}^{\infty}\left[\left(\frac{r}{a}\right)^\ell-\left(\frac{a}{r}\right)^\ell\right]\\ &\quad \times\left(\widetilde{B}^{(s)}_\ell e^{i\ell\theta}+\widetilde{B}^{(s)}_{-\ell}e^{-i\ell\theta}\right).\end{aligned} \tag{48}$$

The magnetic field is determined by (16), so that we have to assume that, to leading order, $B^{(s)}_0$ is proportional to k. Note the correspondence in form between Eqs. (48) and (30).

In the quasistatic limit, for the dipole approximation, the coefficients in (46) are given by (36)–(38) and

$$\begin{aligned}&\frac{J_1(ka)}{Y_1(ka)}\sim-\pi\left(\frac{ka}{2}\right)^2,\quad \frac{J_1(ka)}{Y_0(ka)}\sim\pi\frac{ka}{4\ln(ka)},\\ &\frac{J_0(ka)}{Y_1(ka)}\sim-\pi\frac{ka}{2},\quad \frac{J_0(ka)}{Y_0(ka)}\sim\pi\frac{1}{2\ln(ka)}.\end{aligned} \tag{49}$$

By substituting in (46), for $-1\le\ell,m\le1$, we obtain the homogeneous system:

$$\begin{bmatrix}1+f\frac{\alpha^2}{1-\alpha^2} & -f\frac{e^{i\theta_0}}{a(1-\alpha^2)} & f\frac{e^{2i\theta_0}}{1-\alpha^2}\\ a\,e^{-i\theta_0} & -1 & ae^{i\theta_0}\\ f\frac{e^{-2i\theta_0}}{1-\alpha^2} & -f\frac{e^{-i\theta_0}}{a(1-\alpha^2)} & 1+f\frac{\alpha^2}{1-\alpha^2}\end{bmatrix}\begin{bmatrix}\widetilde{B}^{(s)}_{-1}\\ \frac{2i}{\pi}B^{(s)}_0/k_0\\ \widetilde{B}^{(s)}_1\end{bmatrix}=0. \tag{50}$$

Again, the unknown $B^{(s)}_0/k_0$ is finite at $k_0=0$, as we have assumed that, for small k_0, $B^{(s)}_0\sim k=\alpha k_0$. The determinant of the system (50) is

$$\Delta^{(s)}=-(1-f)^2\neq0,\quad\forall\alpha. \tag{51}$$

This means that the system (50) admits only the trivial solution. Therefore, there is no acoustic band for perfectly conducting cylinders, for s polarization (see Figs. 2, 3, 4, and 5). The minimum value of k is always greater than zero, and we have a complete photonic band gap, which starts at $k=0$ and extends to a cutoff frequency defined by $k_{\min}$ (the lowest value of k when the incident wave vector $\mathbf{k}_0$ follows the boundary of the first irreducible Brillouin zone). This result has been shown by Smith *et al.* [35], in the case of a square array of perfectly conducting cylinders, by using a real space finite difference method.

IV. NUMERICAL RESULTS

A. Convergence and validation of the method

An important question concerning the Rayleigh identity (15) is the number of terms which must be retained when the infinite sum is truncated in order to generate results of a specified accuracy. In Fig. 6 we show the photonic band structure of an array of perfectly conducting cylinders with a low volume fraction, for, respectively, s and p polarization. The bands are shown for several values of the truncation parameter L, where m in Eq. (15) is summed from $-L$ to L. [Hence, the zeros of the determinant of a matrix of size $(2L+1)\times(2L+1)$ are located numerically in order to find allowed values of k for a given $\mathbf{k}_0$. A simple bisection and iterative refinement [36] is adequate to locate these multiple zeros. For

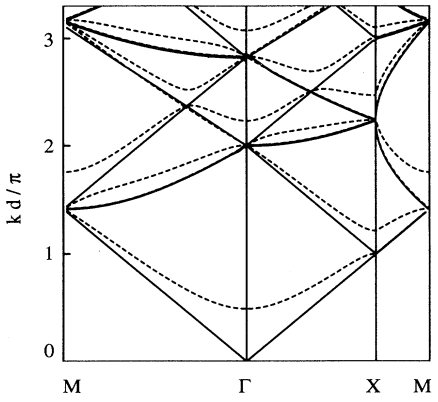

FIG. 2. Photonic band structure of a square array of perfectly conducting cylinders in air, for p (——) and s (- - -) polarization, with $L = 3$. The ratio of the cylinder radii to the array constant is 0.02 (with the area fraction $f = 0.001$).

the Bessel functions and solution of the system (15) we have used the double precision subroutines from AT&T (ftp address netlib.att.com). Care must be taken in the search procedure to avoid k values for which either the lattice sums are singular, i.e., $k = |\mathbf{Q}_h|$ for some reciprocal lattice vector $\mathbf{Q}_h$, or a Bessel function occurring in a denominator in the matrix vanishes.]

It is evident from Fig. 6 that the photonic band structure stabilizes rapidly as L increases, for small f. The band diagrams in Fig. 6 can be compared directly with that shown in Fig. 1 of Ref. [35]. A very satisfactory agreement is evident between the results of these two very different methods. The band diagrams differ significantly in only one small region (the neighborhood of the point M), where the Rayleigh method indicates a definite gap between two branches, which almost touch in the results of Smith *et al.* [35].

The results for a higher area fraction shown in Fig. 7

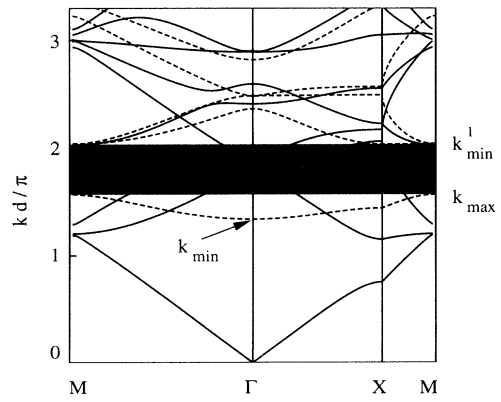

FIG. 3. Photonic band structure of a square array of perfectly conducting cylinders in air, for p (——) and s (- - -) polarization, with $L = 8$. The ratio of the cylinder radii to the array constant is 0.26 (with the area fraction $f = 0.212$). The shaded region is the second in-plane band gap for s polarization.

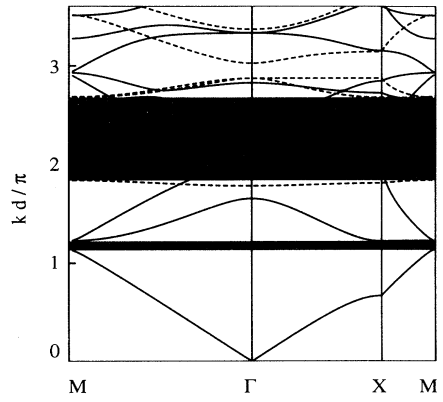

FIG. 4. Photonic band structure of a square array of perfectly conducting cylinders in air, for p (——) and s (- - -) polarization, with $L = 8$. The ratio of the cylinder radii to the array constant is 0.34 (with the area fraction $f = 0.363$). The first shaded region represents the first in-plane band gap for p polarization, while the second shaded region is the second in-plane band gap for s polarization.

illustrate that bigger values of L are needed as the cylinders come close to touching. There is a slight difference in the values of k for $L = 8$ and $L = 12$ along the sixth band, but they coincide elsewhere to graphical accuracy. The convergence of the Rayleigh method for electromagnetic and electrostatic problems is quite similar, and we have found that the table given by Perrins *et al.* [33] for the static case is a reliable guide to the choice of L in Eq. (15).

For an area fraction $f = 0.70$ ($a = 0.472$), the bands for s polarization are almost straight lines (varying by only 10^{-4} across the whole range $M\Gamma XM$) and we obtained the first band at $kd/\pi = 2.7941$, 2.9167, and 2.9173 for $L = 3$, 8, and 12, respectively. Once again, the number of

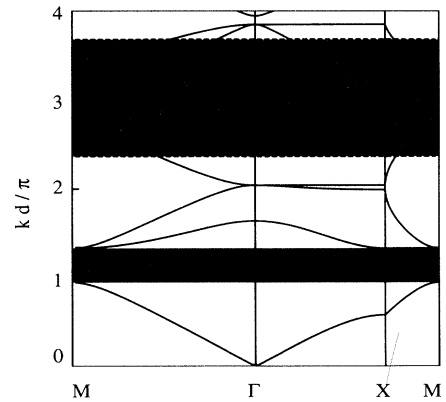

FIG. 5. Photonic band structure of a square array of perfectly conducting cylinders in air, for p (——), and s (- - -) polarization, with $L = 8$. The ratio of the cylinder radii to the array constant is 0.42 (with the area fraction $f = 0.554$). The first shaded region represents the first in-plane band gap for p polarization, while the second shaded region is the second in-plane band gap for s polarization.

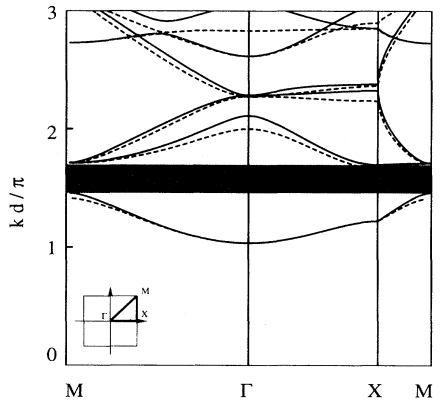

FIG. 6. Photonic band structure of a square array of perfectly conducting cylinders in air, for s polarization, with $L = 1$ (- - -) and $L = 3, 5$ (——). The ratio of the cylinder radii to the array constant is 0.187 (with the area fraction $f = 0.11$). The inset shows the irreducible octant of the first Brillouin zone.

terms specified by Perrins *et al.* [33] for the electrostatic problem is a good guide for the electromagnetic problem.

We prefer not to specify computation times for the results given in this paper, as the code we have used is far from optimized. Most of the computation time is spent in evaluating the lattice sums, which could well be tabulated and stored rather than being reevaluated for each value of cylinder radius (since the S_ℓ^Y do not depend on a). Even without this, the calculation of a photonic band diagram for $L = 8$ takes around 16 h (elapsed time), on a Dec Alpha 800 workstation. Plane-wave calculations of band diagrams typically use supercomputers.

B. Band-gap diagrams for dilute systems

In Fig. 2 we display band structures for square arrays with small radii. As a tends to zero, the p polarization structures tend to the diagrams appropriate to noninteracting plane waves:

$$\frac{\omega}{c} = k = |\mathbf{Q}_h|\,, \tag{52}$$

shown in Fig. 8. Note, however, that near symmetry points such as M, Γ, and X, some bands display localized band gaps, associated with the growth of reflections and the tendency for plane waves to become standing waves. These band gaps shrink as a decreases, giving rise often to degenerate bands. Similar band gaps can occur at the intersection points of bands such as P and R.

The s polarization band structures also tend to the plane-wave forms, but far more slowly than for p polarization. Note, for example, how the fundamental s band has a minimum value $k_{\min}$ which tends very slowly to zero with a, as shown in Fig. 9.

The value of $k_{\min}$ may be estimated as follows. By means of the substitution $\widetilde{B}_\ell^{(s)} = Y_\ell(ka)B_\ell^{(s)}$, the system (15) takes the form

$$\frac{\widetilde{B}_\ell^{(s)}}{J_\ell(ka)} + \sum_{m=-\infty}^{\infty} (-1)^{\ell+m} S_{m-\ell}^Y(k, \mathbf{k}_0) \frac{\widetilde{B}_m^{(s)}}{Y_m(ka)} = 0. \tag{53}$$

Here, for small a, the Bessel functions are approximated by the formulas [32]:

$$J_\ell(ka) \sim \left(\frac{ka}{2}\right)^\ell \frac{1}{\ell!}\,, \quad \ell \geq 0 \tag{54}$$

and

$$\begin{aligned} Y_0(ka) &\sim \frac{2}{\pi} \ln(ka), \\ Y_\ell(ka) &\sim -\frac{1}{\pi}\left(\frac{2}{ka}\right)^\ell (\ell - 1)!, \quad \ell > 0. \end{aligned} \tag{55}$$

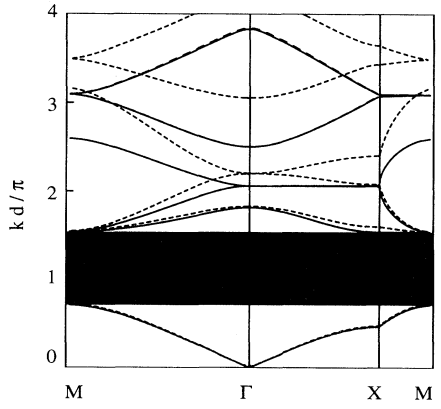

FIG. 7. Photonic band structure of a square array of perfectly conducting cylinders in air, for p polarization, with $L = 3$ (- - -), $L = 8$ (– – –), and $L = 12$ (——). The ratio of the cylinder radii to the array constant is 0.472 (with the area fraction $f = 0.70$).

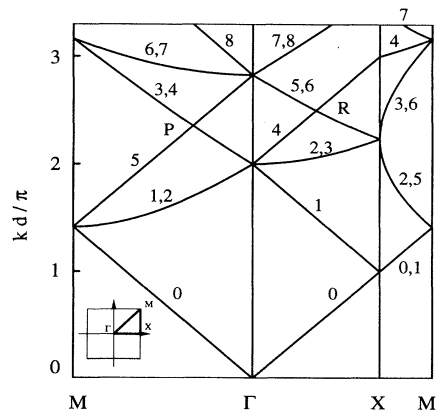

FIG. 8. The set of curves $k = |\mathbf{Q}_h|$, $h = (m, n)$, for a square array. The labels on the curves indicate the pairs (m, n) as follows: $0 = (0, 0)$, $1 = (-1, 0)$, $2 = (0, -1)$, $3 = (0, 1)$, $4 = (1, 0)$, $5 = (-1, -1)$, $6 = (-1, 1)$, $7 = (1, -1)$, and $8 = (1, 1)$. The inset shows the irreducible octant of the first Brillouin zone.

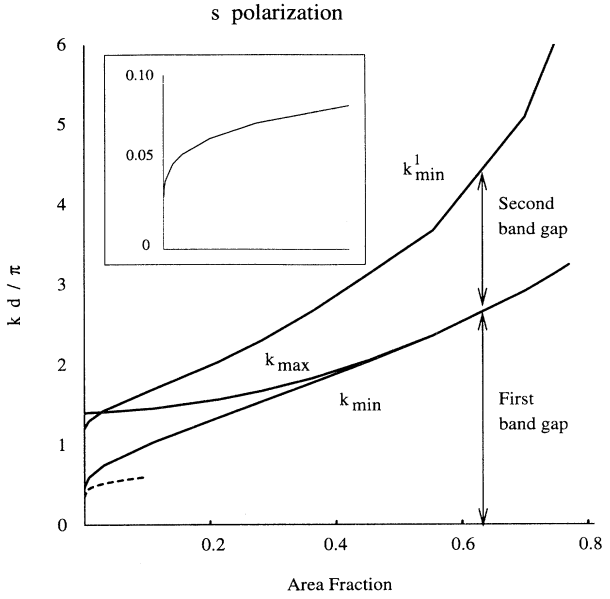

FIG. 9. The minimum ($k_{\min}$) and maximum ($k_{\max}$) values of k along the acoustic band, as a function of area fraction of the square array. $k^1_{\min}$ represents the minimum value of k along the first optical band, as a function of area fraction. ($k_{\min}$, $k_{\max}$, and $k^1_{\min}$ are defined in Fig. 3.) The dashed curve represents $k_{\min}$ given by the formula (61). The inset displays the the difference between $k_{\min}$ and the formula (61), for $10^{-6} \leq f \leq 10^{-3}$.

The minimum of the lowest band for s polarization is attained at the Γ point, so that we consider the case $\mathbf{k}_0 = 0$. At this point, for $k \neq K_h$, $\forall h$, the lattice sums S^Y_ℓ are finite. Consequently, for small a we have $\widetilde{B}^{(s)}_\ell = 0$, $\forall \ell \neq 0$. The equation for $\widetilde{B}^{(s)}_0$ is

$$\left[1 + \frac{S^Y_0(k,0)}{Y_0(ka)}\right] \widetilde{B}^{(s)}_0 = 0, \tag{56}$$

and we may have $\widetilde{B}^{(s)}_0 \neq 0$ if

$$\frac{2}{\pi} \ln(ka) + S^Y_0(k,0) = 0. \tag{57}$$

From [16], we obtain the lattice sum S^Y_0 as

$$S^Y_0(k,0) J_0(k\xi) = -Y_0(k\xi) + \frac{4}{k^2 A} - \frac{4}{A} \sum_{h \neq 0} \frac{J_0(K_h \xi)}{K_h^2 - k^2}, \tag{58}$$

where $\boldsymbol{\xi}$ is a vector inside the unit cell. We have proved in [16] that the lattice sums S^Y_ℓ are independent of ξ, and we choose

$$\xi = d = \min_{j=1,2} \{|\hat{\mathbf{e}}_j|\}. \tag{59}$$

Note that (59) may be used for a general array. For a square or hexagonal array the fundamental translation vectors have the same length, $|\hat{\mathbf{e}}_1| = |\hat{\mathbf{e}}_2| = d$.

The series in (58) converge as $K_h^{-2.5}$ and we will denote its sum by $\sigma(k)$. In the limit of very small a, $k_{\min}$ is also small and we may assume that Eq. (57) may be written in the form

$$\frac{2}{\pi} \ln\left(\frac{a}{d}\right) + \frac{4}{k^2_{\min} A} - \frac{4}{A} \sigma(k_{\min}) = 0. \tag{60}$$

If we approximate $\sigma(k_{\min})$ by $\sigma(0)$, we obtain

$$k_{\min} \sim \left[-\frac{A}{2\pi} \ln(a/d) + \sigma(0)\right]^{-1/2}. \tag{61}$$

Note how steeply this function tends to zero with a (Fig. 9, plotted for the square array, for which $\sigma(0) \approx 0.042$).

C. Band-gap diagrams for concentrated systems

In Figs. 3, 4, and 5 we show band gap diagrams for a ranging from 0.26 to 0.42. Our numerical results show the first in-plane gap, for p polarization, opening up as $a/d > 0.30$ (see Figs. 4 and 5). We have analyzed particularly the dependence of the gap size, defined as the ratio of the gap width to the midgap frequency, on the area fraction (Fig. 10). Note how this gap tends to increase strongly as $a \to 0.5$, or $f \to \pi/4$ (the area fraction for touching cylinders).

For s polarization we note the existence of a first in-plane band gap between $k = 0$ and a cutoff frequency given by $k_{\min}$. The dependence of $k_{\min}$ on the area fraction is shown in Fig. 9. Note how the maximum and

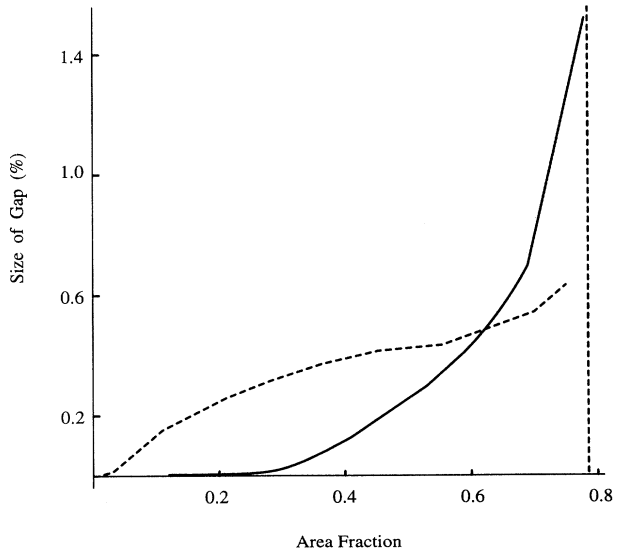

FIG. 10. Size of the two-dimensional photonic band gap in a square array of perfectly conducting cylinders in air, as a function of the area fraction. The first in-plane band gap for p polarization (——) and the second in-plane band gap for s polarization (- - -) are shown. The size of the gap is defined as the ratio of the gap width to the midgap frequency. The vertical dashed line indicates the area fraction for touching cylinders ($f = \pi/4$).

minimum values of k for the lowest s polarization band tend to a common value as f increases, with this band tending to a straight line.

There is a second band gap, for s polarization, opening up for small area fractions $f \gtrsim 0.01$ (see Fig. 3). The size of this band gap as a function of area fraction is displayed in Fig. 10. Both the first and second gaps open with increasing area fraction, and both may well diverge as the cylinders approach touching.

An interesting feature of the dispersion curves for s polarization is that these curves tend to straight lines, which are degenerate, apart from the lowest band. We believe that the flatness of the s polarization bands is due to their corresponding to cavity modes of the space between the cylinders, and thus their frequency being independent of the excitation conditions (i.e., of $\mathbf{k}_0$).

The first in-plane band gap for p polarization appears and develops inside the first in-plane band gap for s polarization, accordingly defining a common band gap for both polarizations (this common band gap exists for cylinder radii larger than 0.30). The appearance of the first p polarization band gap is associated with a pronounced flattening of the second p band in the region XM.

D. Photonic band structure of hexagonal arrays

In Fig. 11 we display the free space dispersion curves for hexagonal symmetry, and in Fig. 12 we give the dispersion curves for a hexagonal array of perfectly conducting cylinders of radius $a = 0.34$, in air. We used a truncation order $L = 8$ in (15). For p polarization, from the values of k along the acoustic band close to the Γ point, we have obtained the value of the slope $\alpha \approx 0.838\,77$, giving an effective dynamic refractive index $\mathcal{N} \approx 1.1922$. The area fraction is $f = 2\pi a^2/\sqrt{3} = 0.4194$, and from (42) we have $\mathcal{N}_d = 1.1914$. Note the good agreement between the value of $\mathcal{N}$ for a higher truncation order, and $\mathcal{N}_d$ from the dipole approximation. The Maxwell Garnett formula (45) gives the value $N_d = 1.5635$, which differs significantly from $\mathcal{N}_d$.

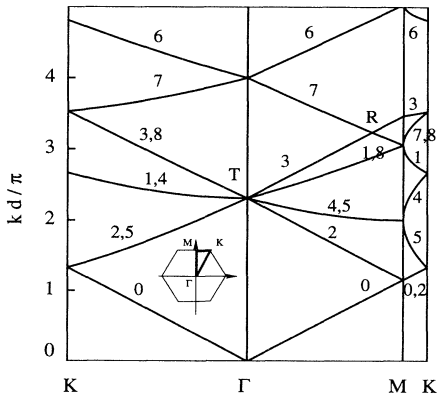

FIG. 11. The set of curves $k = |\mathbf{Q}_h|$, $h = (m,n)$, for a hexagonal array. The labels on the curves indicate the pairs (m,n) as follows: $0 = (0,0)$, $1 = (-1,0)$, $2 = (0,-1)$, $3 = (0,1)$, $4 = (1,0)$, $5 = (-1,-1)$, $6 = (-1,1)$, $7 = (1,-1)$, and $8 = (1,1)$. The inset shows the irreducible part of the first Brillouin zone.

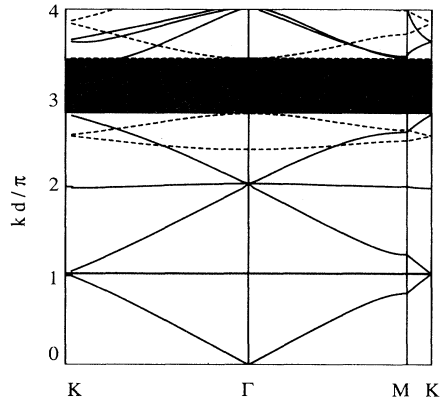

FIG. 12. Photonic band structure of a hexagonal array of perfectly conducting cylinders in air, for p (——) and s (- - -) polarization, with $L = 8$. The ratio of the cylinder radii to the array constant is 0.34 (with the area fraction $f = 0.419$). The first shaded region represents the first in-plane band gap for p polarization, while the second shaded region is the second in-plane band gap for s polarization.

Note that the fundamental p polarization band gap is much smaller in Fig. 12 than in Fig. 4. Another significant difference is that the photonic band structures in the regions $K\Gamma$ and ΓM are much more similar for the hexagonal array than for the square array. We also note the absence of band crossings and band separations, other than at symmetry lines. Figure 12 retains no sign of the intersection point at R in Fig. 11.

The first s polarization band gap is significantly larger for the hexagonal array than for the square array. Note that the changes to band arrangement near the point T (in Fig. 11) are much more pronounced for s polarization than for p polarization. For s polarization the lower bands passing through T become associated with the fundamental band, while the upper bands move off to higher k values. A curious feature of both the s and p structures in Fig. 12 is the existence of flatbands; we plan to investigate the physics of these in more detail.

V. CONCLUSIONS

We have studied the propagation of electromagnetic waves in arrays of perfectly conducting cylinders, concentrating on two aspects of their propagation characteristics. First, we have used the lowest p polarization band to define an effective refractive index and have shown that, perhaps counterintuitively, this quantity *does not* agree with the effective refractive index which results from electrostatic calculations. We do not interpret this as meaning that over 100 years of results based on homogenization procedures devised by Lorenz and Lorentz are incorrect, but rather that the case of perfectly conducting inclusions represents a special, isolated case in homog-

enization theory. Second, we have studied the photonic band diagrams for both s and p polarizations over almost the whole range of area fractions. For dilute systems, the diagrams tend in a very satisfactory way to the freely propagating plane-wave diagram, although with very interesting polarization differences. For concentrated systems, the polarization effects are quite striking, with the s polarization bands becoming very flat, while the p polarization bands remain nontrivial. We note the existence of a common band gap between s and p polarizations for cylinder radii larger than 0.30.

We are currently extending our studies to arrays of dielectric circular cylinders, and also to elliptical cylinders. Parallel investigations of lattices of spheres are in course.

ACKNOWLEDGMENTS

This work was undertaken while one of the authors (N.A.N.) was supported by an Australian Research Council Grant. This body also provided computing facilities. The Science Foundation for Physics within the University of Sydney is also acknowledged.

[1] S. John, Phys. Rev. Lett. **58**, 2486 (1987).
[2] E. Yablonovitch, T. J. Gmitter, and K. M. Leung, Phys. Rev. Lett. **67**, 2295 (1991).
[3] S. Y. Lin and G. Arjavalingam, Opt. Lett. **18**, 1666 (1993).
[4] K. M. Leung and Y. F. Liu, Phys. Rev. Lett. **65**, 2646 (1990).
[5] Z. Zhang and S. Satpathy, Phys. Rev. Lett. **65**, 2650 (1990).
[6] K. M. Ho, C. T. Chan, and C. M. Soukoulis, Phys. Rev. Lett. **65**, 3152 (1990).
[7] H. S. Sözüer, J. W. Haus, and R. Inguva, Phys. Rev. B **45**, 13 962 (1992).
[8] P. R. Villeneuve and M. Piché, J. Mod. Opt. **41**, 241 (1994).
[9] P. R. Villeneuve and M. Piché, Prog. Quantum Electron. **18**, 153 (1994).
[10] J. B. Pendry and A. MacKinnon, Phys. Rev. Lett. **69**, 2772 (1992).
[11] Lord Rayleigh, Philos. Mag. **34**, 481 (1892).
[12] N. A. Nicorovici, R. C. McPhedran, and R. Petit, Phys. Rev. E **49**, 4563 (1994).
[13] N. A. Nicorovici, and R. C. McPhedran, Phys. Rev. E **50**, 3143 (1994).
[14] R. C. McPhedran, N. A. Nicorovici, and R. Petit, in *Progress in Electromagnetic Research Symposium Proceedings (PIERS'94)*, edited by B. Arbesser-Rastburg *et al.* (Kluwer, Dordrecht, The Netherlands, 1994), on CD-ROM.
[15] R. C. McPhedran and D. H. Dawes, J. Electromagn. Waves Appl. **6**, 1327 (1992).
[16] S. K. Chin, N. A. Nicorovici, and R. C. McPhedran, Phys. Rev. E **49**, 4590 (1994).
[17] L. C. Botten, R. C. McPhedran, and N. A. Nicorovici, in *Progress in Electromagnetic Research Symposium Proceedings (PIERS'94)*, edited by B. Arbesser-Rastburg *et al.* (Kluwer, Dordrecht, The Netherlands, 1994), on CD-ROM.
[18] N. A. Nicorovici, R. C. McPhedran, and Bao Ke-Da, Phys. Rev. E **51**, 690 (1995).
[19] P. P. Ewald, Ann. Phys. (Leipzig) **64**, 253 (1921).
[20] E. Sanchez-Palencia, *Non-homogeneous Media and Vibration Theory*, Lecture Notes in Physics Vol. 127 (Springer-Verlag, Berlin, 1980).
[21] *Macroscopic Properties of Disordered Media*, edited by R. Burridge, S. Childress, and G. Papanicolaou, Lecture Notes in Physics Vol. 154 (Springer-Verlag, Berlin, 1982).
[22] *Homogenization and Effective Moduli of Materials and Media*, edited by J. L. Ericksen *et al.*, The IMA Volumes in Mathematics and Its Applications Vol. 1 (Springer-Verlag, New York, 1986).
[23] *Homogenization Techniques for Composite Media*, edited by E. Sanchez-Palencia and A. Zaoui, Lecture Notes in Physics Vol. 272 (Springer-Verlag, Berlin, 1987).
[24] N. Bakhvalov and G. Panasenko, *Homogenisation: Averaging Processes in Periodic Media* (Kluwer, Dordrecht, 1989).
[25] *Composite Media and Homogenization Theory*, edited by G. Dal Maso and G. F. Dell'Antonio, Progress in Nonlinear Differential Equations and their Applications Vol. 5 (Birkhäuser, Boston, 1991).
[26] Proceedings of the Third International Conference on Electrical Transport and Optical Properties of Inhomogeneous Media (ETOPIM 3) [Physica A **207**, Nos. 1–3 (1994)].
[27] D. Felbacq, G. Tayeb, and D. Maystre, J. Opt. Soc. Am. A **11**, 2526 (1994).
[28] K. M. Lo, R. C. McPhedran, I. M. Basett, and G. W. Milton, IEEE J. Lightwave Technol. **12**, 396 (1994).
[29] W. K. H. Panofsky and M. Phillips, *Classical Electricity and Magnetism*, 2nd ed. (Addison-Wesley, Reading, MA, 1962).
[30] C. Kittel, *Introduction to Solid State Physics* (Wiley, New York, 1986).
[31] R. Landauer, in *Electrical Transport and Optical Properties of Inhomogeneous Media*, edited by J. C. Garland and D. B. Tanner (American Institute of Physics, New York, 1978).
[32] *Handbook of Mathematical Functions with Formulas, Graphs and Mathematical Tables*, edited by M. Abramowitz and I. A. Stegun (Dover, New York, 1972).
[33] W. T. Perrins, D. R. McKenzie, and R. C. McPhedran, Proc. R. Soc. London Ser. A **369**, 207 (1979).
[34] R. C. McPhedran and D. R. McKenzie, Appl. Phys. **23**, 223 (1980).
[35] D. R. Smith *et al.*, Appl. Phys. Lett. **65**, 645 (1994).
[36] W. H. Press, S. A. Teukolsky, W. T. Vetterling, and B. P. Flannery, *Numerical Recipes in FORTRAN* (Cambridge University Press, New York, 1992).